Int J CARS (2014) 9:11–20
DOI 10.1007/s11548-013-0908-5

REVIEW ARTICLE

Surgical planning tool for robotically assisted hearing aid implantation

Nicolas Gerber · Brett Bell · Kate Gavaghan · Christian Weisstanner · Marco Caversaccio · Stefan Weber

Received: 1 February 2013 / Accepted: 3 June 2013 / Published online: 14 June 2013

Abstract
Purpose For the facilitation of minimally invasive robotically performed direct cochlea access (DCA) procedure, a surgical planning tool which enables the surgeon to define landmarks for patient-to-image registration, identify the necessary anatomical structures and define a safe DCA trajectory using patient image data (typically computed tomography (CT) or cone beam CT) is required. To this end, a dedicated end-to-end software planning system for the planning of DCA procedures that addresses current deficiencies has been developed.
Methods Efficient and robust anatomical segmentation is achieved through the implementation of semiautomatic algorithms; high-accuracy patient-to-image registration is achieved via an automated model-based fiducial detection algorithm and functionality for the interactive definition of a safe drilling trajectory based on case-specific drill positioning uncertainty calculations was developed.
Results The accuracy and safety of the presented software tool were validated during the conduction of eight DCA procedures performed on cadaver heads. The plan for each ear was completed in less than 20 min, and no damage to vital structures occurred during the procedures. The integrated fiducial detection functionality enabled final positioning accuracies of 0.15 ± 0.08 mm.
Conclusions Results of this study demonstrated that the proposed software system could aid in the safe planning of a DCA tunnel within an acceptable time.

Keywords Surgical planning · Hearing aid implantation · Robotically assisted microsurgery · Segmentation

N. Gerber (✉) · B. Bell · K. Gavaghan · S. Weber
ARTORG Center for Biomedical Engineering Research,
University of Bern, Murtenstrasse 50,
3010 Bern, Switzerland
e-mail: nicolas.gerber@artorg.unibe.ch
www.artorg.unibe.ch

C. Weisstanner
Institute of Diagnostic and Interventional Neuroradiology,
University Hospital of Bern (Inselspital), 3010 Bern,
Switzerland

M. Caversaccio
Department of Ear, Nose and Throat Diseases (ENT),
Head and Neck Surgery, University Hospital
of Bern (Inselspital), 3010 Bern, Switzerland

Introduction

Implantable hearing aids are able to restore hearing in moderately and profoundly deaf people. The majority of devices, such as the cochlear implant (CI) and the direct acoustical cochlea stimulator (DACS), require access to the middle and/or inner ear, created by drilling in the lateral skull base. The most invasive component of the procedure is the mastoidectomy during which a large cavity is milled out of the mastoid, in order to locate and preserve risk structures such as nerves.

Because the mastoidectomy (⌀30–40 mm) is much larger than is physically required to insert implantable hearing aids, several surgical strategies have been proposed to reduce invasiveness [1,2]. A percutaneous or direct cochlear access (DCA) approach was introduced by Warren et al. [3], who suggested that access could be gained by drilling a tunnel only slightly larger than the implant in diameter (1–2 mm in case of CI) with the aid of image guidance. The drilled trajectory would originate on the outer surface of the mastoid, pass through the facial recess, and terminate in the middle ear cavity in the region of the round or oval window.

Feasibility of an image-guided DCA was previously investigated, and it was found that a drilling accuracy of at least 0.5 mm would be required to safely drill through the facial recess without damaging any surrounding structures [4]. To achieve such accuracy, a robotically assisted procedure which overcomes the inability to precisely position the surgical drill using hand held instruments [5] was suggested [6–10]. The safe and effective conduction of an image guided, robotically assisted DCA procedure, strongly relies on the quality of the surgical plan and the accuracy at which the surgical plan can be registered to the physical patient intraoperatively.

The primary objective of the surgical plan is the definition of a safe path along which a surgical drill could pass without penetrating any sensitive structure. These structures include the facial nerve, the chorda tympani, the external auditory canal wall and the ossicles. The facial nerve controls all movement of the ipsilateral face and any injury would result in temporary or permanent paralysis of half of the patient's face. Damage to the chorda tympani would cause temporary or permanent loss of taste of the ipsilateral tongue. Possible future infection could be caused by a breach of the external auditory canal. Looking from the mastoid surface to the cochlea, all of the aforementioned structures are contained within a window, typically 1.0–3.5 mm in diameter [11], through which the trajectory must also pass. As a result, preoperative planning software solutions, which allow for the segmentation of critical structures, are needed to safely and effectively plan DCA procedures.

Trajectory planning on 2D image slices is difficult due to poor representation of the spatial arrangements of anatomical structures. 3D environments greatly facilitate this process [12–15]; however, segmentation of the preoperative image data is required in order to create 3D surface models of the anatomy of interest. Several segmentation algorithms have been proposed and are reviewed in [16,17]. However, very few of these algorithms have been implemented and verified in a preoperative planning software tool. Automatic segmentation of the aforementioned anatomical structures for DCA procedure planning was described by Noble et al. [14] using an atlas-based solution. One important underlying assumption of atlas-based identification method is that the image volumes used to create the atlas have similar topology. As a result, errors in segmentation may occur in cases of malformed ears. In addition, automatic algorithms remove the surgeon from the segmentation process, thus reducing feedback regarding segmentation margins. As a result, a framework which allows visualisation of the segmentation output for verification, as well as tools for the possible alteration of segmentation results, is required for a robust preoperative planning tool suitable for clinical use.

Automatic trajectory definition and optimisation for DCA procedures based on 3D modelled structures, user-supplied structure preservation weightings and general system accuracy have been previously proposed [11]. Optimal trajectory positioning should not, however, be determined on the basis of anatomy alone, and in such algorithms, case-specific error, patient indications, surgeon preferences and experience and local regulations have not been considered. Additionally, adjustments to the automatically defined trajectories by the surgeon are not possible. A tool that can provide a case-specific prediction of safety margins and enables surgeons to define the optimal trajectory based on all of the available patient information is yet to be described.

For conduction of the defined surgical plan, a planning tool for DCA must provide functionality for registering the plan to the patient with an accuracy approximately 10 times better (0.1–0.2 mm) than that available in commercial navigation systems. It has been shown that the target registration error (TRE), the Euclidean distance between points in the physical space and corresponding points from the image space transformed via the registration process, depends on the fiducial localisation error (FLE) [18]. Thus, localisation of the fiducial markers in the image plays an important role in the achievement of accuracy required to complete a successful DCA. Automated fiducial detection, which eliminates user variability, has been widely reported in image-guided neurosurgery and ear, nose and throat surgery [19–26]; however, these methods provide accuracies insufficient for DCA procedures.

For the facilitation of middle ear access through a minimally invasive DCA procedure, a surgical planning tool which enables the surgeon to define landmarks for patient-to-image registration, identify the necessary anatomical structures and define a safe DCA trajectory using patient image data (typically computed tomography (CT) or cone beam CT (CBCT)) is required. However, to our knowledge, no end-to-end solution is available. To this end, we have developed a dedicated end-to-end software planning system for the planning of DCA procedures that addresses current deficiencies.

The proposed software tool, including methods of fiducial localisation, structure segmentation, trajectory definition and error prediction, is described within this work. In addition, the results of an initial validation of the software, as conducted during the drilling of DCA tunnels for CI implantation in cadaver heads, are presented.

Methods

The proposed planning software tool was designed to interface with the robotic system described in Bell et al. [27]. The five degrees of freedom (DoF) serial kinematic surgical robot system was developed as a dedicated solution for DCA cochlear implantation surgery. The robotic arm contains a six DoF force torque sensor in its wrist (Mini40, ATI, USA),

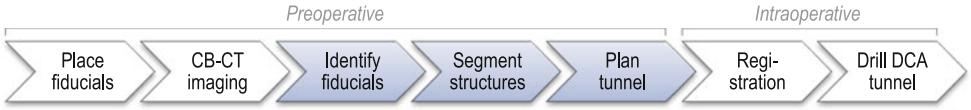

Fig. 1 Clinical workflow using the proposed software planning system for DCA surgery. Steps highlighted in *blue* are performed preoperatively using the proposed planning software system

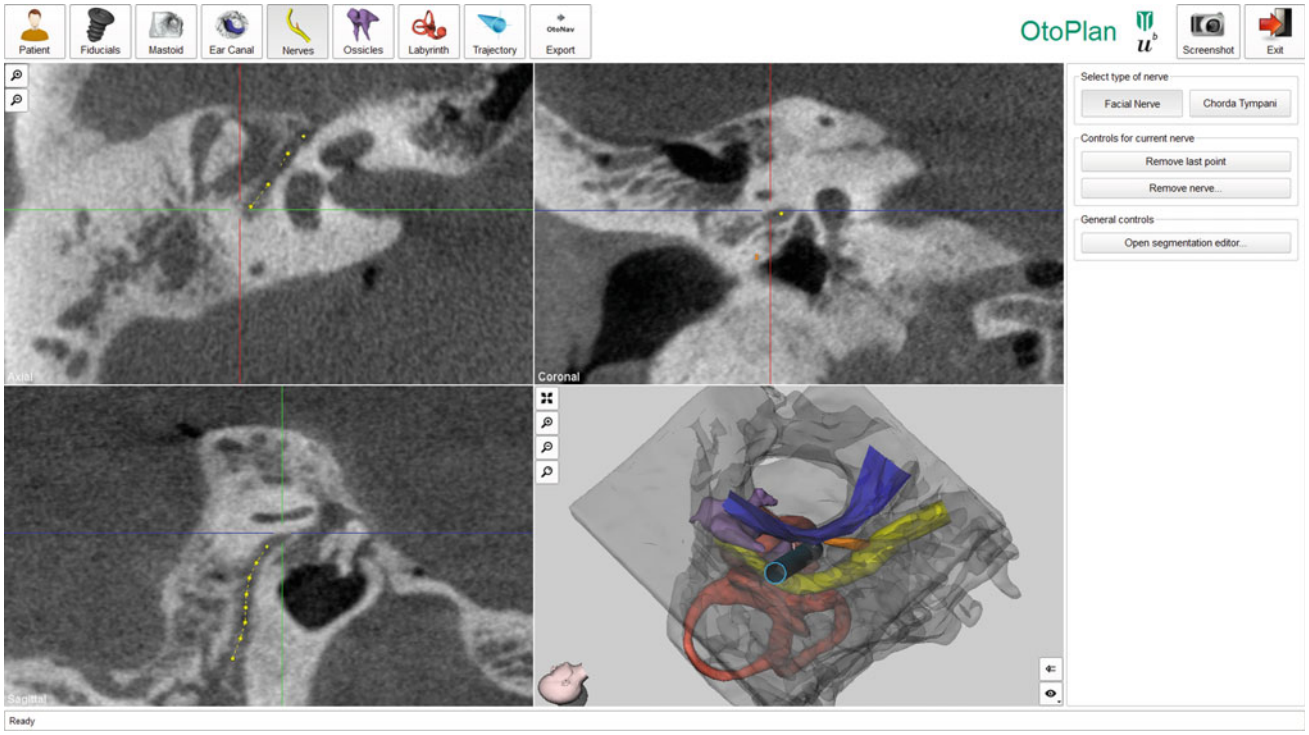

Fig. 2 User interface of the proposed planning software system showing a completed plan

which allows the user to manipulate the end effector within the robot's workspace through admittance control. Navigation is provided by a high-precision optical tracking system (CamBar B1, Axios 3D GmbH, Germany) which is attached to the robot's base and operates at a distance of 150–350 mm from the situs. It tracks active tracking markers attached to the tool and the patient within a cubic workspace of approximately 200 mm × 200 mm × 200 mm with an accuracy of 0.05 mm. Patient-to-image registration is achieved through pair point matching of bone implanted ∅1.5 × 3 mm titanium surgical screws (M-5220.03, Medartis, Switzerland), which are localised in the patient coordinate system through a semi-automatic ball-in-cone positioning method [28]. The robot is designed to autonomously drill a preoperatively planned trajectory through the mastoid to the middle ear following the workflow depicted in Fig. 1.

Initially, at least three (typically four) fiducial screws are implanted into the patient's temporal bone to provide correspondence between the patient and the image data set. Fiducials are inserted around the external auditory canal at the zygomatic process, the mastoid process and two additional positions approximately equidistant on the opposite side of the external auditory meatus. Preoperative images of the patient's mastoid are then acquired using a CBCT system (i.e. ProMax 3D Max, Planmeca, Finland) in high-resolution mode (0.15 mm × 0.15 mm × 0.15 mm).

After loading the patient image data, a plan is performed in three primary steps: the detection of fiducial marker positions for patient-to-image registration, the segmentation of relevant anatomical structures and the definition of a trajectory. These three steps are described below in detail. Once the plan is complete, it is saved and exported for use by the robotic system described above. Finally, the patient is registered to the plan intraoperatively, and the DCA is drilled by the robotic system.

The proposed planning software system (see Fig. 2) was developed using the C++ programing language and open source libraries including: Qt (Digia, Helsinki, Finland), Open Inventor (Coin3D, Kongsberg, Norway), the DICOM Toolkit (DCMTK, OFFIS computer science institute, Germany), the Visualization Toolkit (VTK, Kitware Inc., USA) and the Insight Segmentation and Registration Toolkit (ITK,

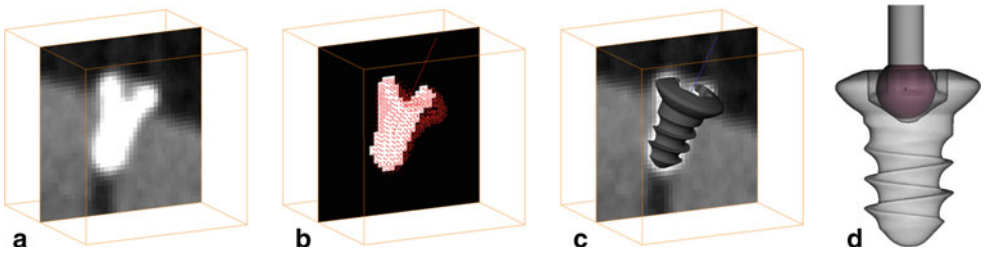

Fig. 3 Fiducial detection workflow in the image: cropped sub-volume (**a**); extracted features with binary sub-volume (**b**); and co-registered fiducial model and image (**c**). Ball-in-cone representation (**d**)

Kitware Inc., USA). It was designed to be run on a standard laptop computer by medical staff.

Fiducial localisation

To enable the drilling of a DCA tunnel with accuracy greater than 0.5 mm, a target registration error of less than 0.2 mm is required. In order to achieve such high accuracy, an automated technique that removes user variability was developed [28].

Within the image, the screw location must be defined as the position at which the robotic system's registration tool sits in the conical indent in the fiducial screw head (refer to Fig. 3d). An initial coarse localisation of each fiducial screw is manually defined with a user-supplied single selection. Thereafter, the exact registration position of the fiducial is determined automatically by the proposed planning software system using the following methodology (see Fig. 3):

1. A small sub-volume encompassing each screw is cropped from image volume data.
2. Features corresponding to the boundary of the fiducial screw are extracted by applying a gradient magnitude filter followed by thresholding of the sub-volume.
3. A threshold is applied to the gradient magnitude in order to extract the voxels located at the boundary of the fiducial screw.
4. A coarse registration of the 3D surface model to the corresponding binary sub-volume is computed using their respective centroids and principal axes.
5. The 3D surface model is iteratively matched to the extracted features via a standard iterative closest point matching algorithm.
6. The position of the screw, transformed to the calibrated registration tool position within the screw's indent, is returned.

This methodology was verified on phantoms with clinically relevant fiducial and target locations. The fiducial localisation in the image ($\mathrm{FLE_{im}}$) was found to have a ground truth error of 0.153 mm $\pm$ 0.061 mm ($N = 30$) and, when used in conjunction with the automatic fiducial detection technique on the patient ($\mathrm{FLE_{pat}} = 0.046\,\mathrm{mm} \pm 0.029\,\mathrm{mm}$), a mean TRE of 0.101 mm $\pm$ 0.40 mm ($N = 144$). For a more detailed description of the registration methodology and its verification, we direct the reader to Gerber et al. [28].

Anatomical structure segmentation

The definition of a safe DCA trajectory initially requires 3D segmented models of the relevant anatomical structures of the outer and middle ear. The required structures include the mastoid for definition of the trajectory entry position; the round window or the oval window as a target for the drilled trajectory; and the auditory ear canal wall, the facial nerve, the chorda tympani and the ossicles as anatomy to preserve during the drilling process.

A semiautomatic approach to segmentation was adopted in order to allow structures to be quickly and easily segmented whilst allowing the operator to maintain control over the segmentation margins and segmentation verification.

After loading the patient's images, a 3D surface model of the mastoid is created using three steps. Firstly, the user defines a lower and an upper threshold to select the bony structures in the image data set. Voxels with a value inside the defined range are displayed with a red overlay mask (see Fig. 4). Secondly, a box is delimited to select the volume of interest, encompassing the mastoid surface, the external auditory canal and the middle ear and inner ear. This step reduces the time required for segmentation and is necessary because the mastoid is highly pneumatised and therefore results in a large surface area. Subsequent image processing operations are performed in the volume of interest, with VTK filters, using the selected voxels. To smooth the image, a Gaussian filter is applied ($\sigma = 0.4$ in x, y and z directions). Image thresholding is performed using previously user-defined lower and upper thresholds. The resulting binary mask is further processed with an island removal filter. The marching cube algorithm [29] is used to create the 3D surface model before usage of a windowed sinc smoothing filter.

The posterior external auditory canal wall (EAC) is segmented from four user-supplied mouse clicks. The EAC is

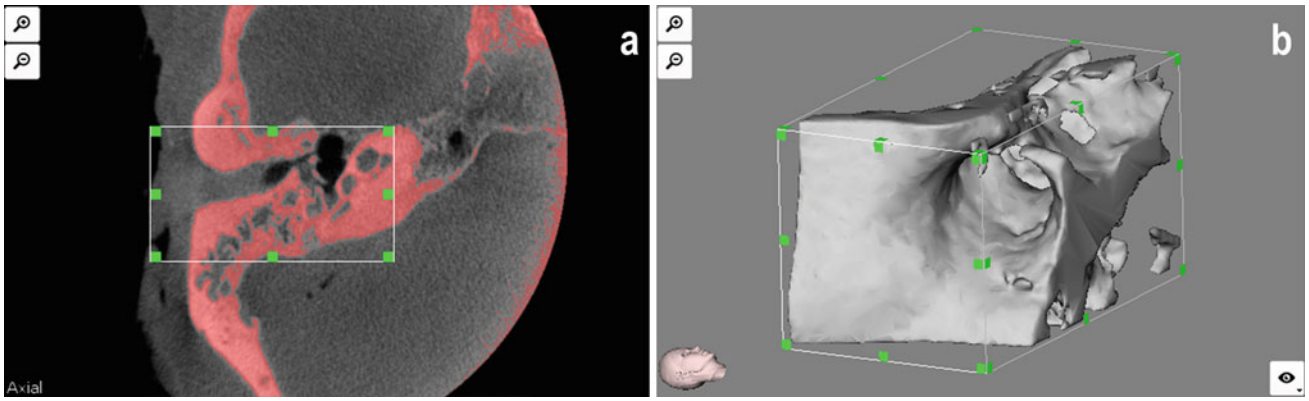

Fig. 4 Mastoid segmentation with selected *red* overlay (**a**). 3D surface model of the mastoid region (**b**)

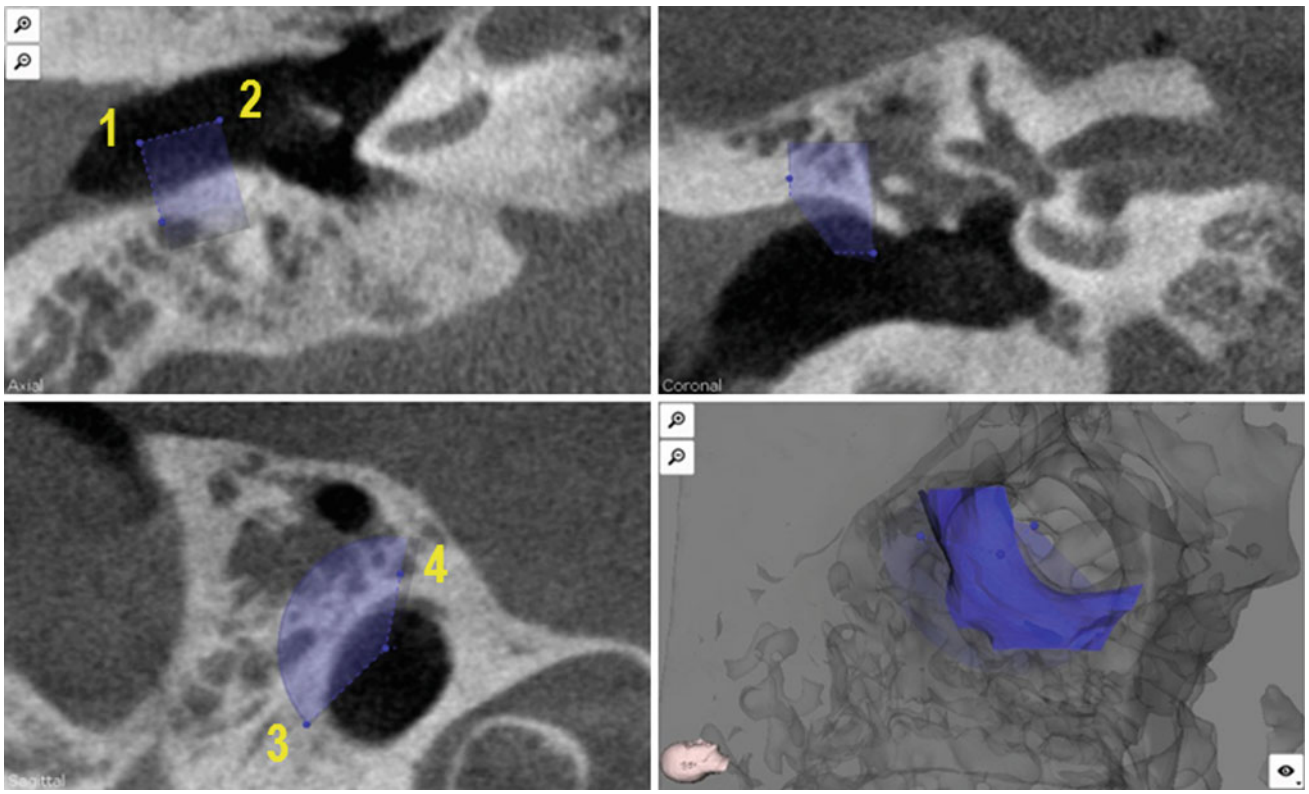

Fig. 5 External auditory canal wall segmentation using 4 points and a defined threshold

first located on the axial view, and its axis is defined by selecting two points (points one and two on Fig. 5). The software displays the sagittal plane that passes through the middle of the axis. The user is then prompted to define an angle incorporating the desired wall portion to segment by clicking points three and four on the sagittal view. The EAC wall is automatically computed using a customised algorithm based on a threshold intensity value. Starting from the EAC's axis moving radially in the defined region, the wall is located when the voxel intensity reaches the specified threshold. The threshold is initially defined as the value used to segment the mastoid; however, alteration of its value can be performed in the user interface. Finally, a 3D surface is computed using the resulting point cloud by means of the VTK surface reconstruction filter.

Segmentations of the facial nerve and chorda tympani are performed in two steps. In a first step, the approximate centreline of each nerve is determined by connecting a number of user-supplied mouse clicks (approximately 10) along the nerve on any of the standard axial, coronal and sagittal planes (see Fig. 6a).

In a second step, curved planar reconstruction (CPR) [30] is used to create a panoramic view of the nerve along the previously selected centreline (see Fig. 6b). A first identification

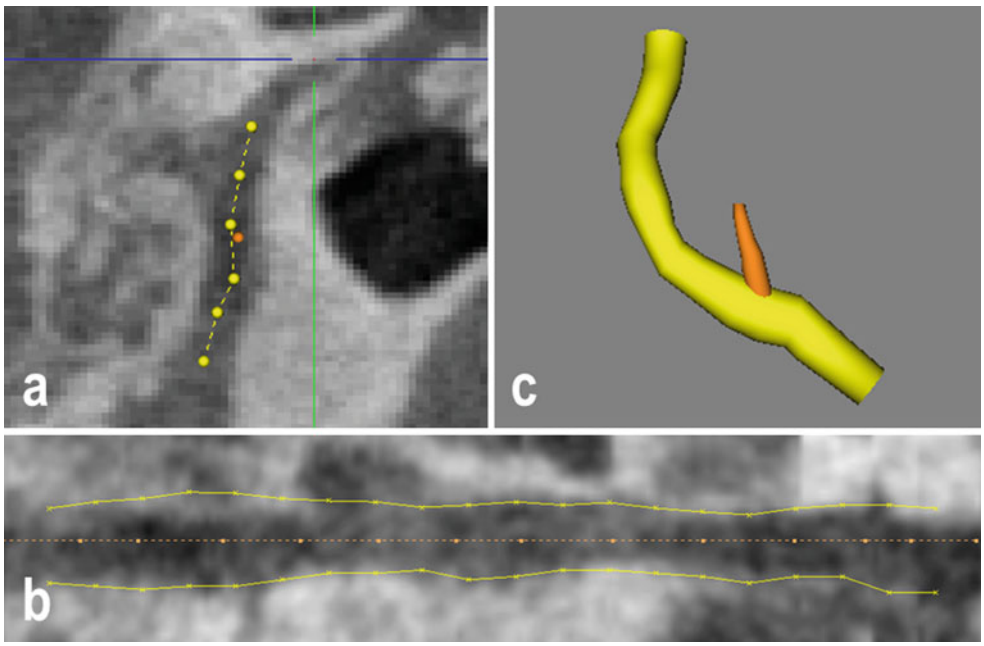

Fig. 6 Interactive drawing of the facial nerve and chorda tympani centrelines (**a**). Curved planar reconstruction (CPR) along the facial nerve's centreline (**b**). 3D surface model of the facial nerve and chorda tympani (**c**)

of the nerve's borders is automatically suggested to the user. Starting from equally spaced points on the centreline and moving up and down until a predefined threshold intensity is reached, the boundary of the nerve is found. Alteration of the borders is left to the user, who can drag and drop any drawn border points. Furthermore, the CPR plane can be manually rotated along the nerve's centreline for visual inspection in the 3D volume. Finally, the 3D surface model of the nerve is created by connecting cylinders based on the CPR segmentation (see Fig. 6c).

The segmentation of the ossicles is divided into segmentation of the incus and malleus, and segmentation of the stapes. A region growing algorithm with connected thresholds criterion is initiated after point selection on the incus or malleus (see Fig. 7). The thresholds can be modified in the graphical user interface. Similarly to the mastoid, a marching cubes algorithm [29] is then used to create the 3D surface model of the structures.

The stapes is manually segmented using three user selected (clicked) landmarks. First, the tip of the incus lenticular process is selected. Secondly, the anterior border of the oval window is selected. Thirdly, the posterior border of the oval window is defined. A cone shape is created using these three landmarks to define the volume region of the stapes.

Tunnel definition

Having the necessary anatomical structures modelled, a trajectory can be defined. The target, typically the middle of the round window for a CI or the middle of the oval window for a DACS implant, is manually selected on the image data set by a single mouse click. Subsequently, the entry point is manually designated on the surface of the mastoid, by a single mouse click, in order to establish a suitable tunnel avoiding the previously modelled structures. The trajectory is optimised by manually dragging the selected entrance point along the mastoid surface until sufficient distance to the anatomical structures is found or until the surgeon determines that the facial recess is of insufficient size for robotic surgery eligibility. To aid the surgeon in the determination of a safe trajectory, predicted error pertaining to the DCA procedure is calculated and displayed as a 3D model around the planned trajectory. In addition, safety margins, measured from the surface of the trajectory model (including error) to anatomical structures, are computed and displayed. The predicted error and the safety margins are recomputed and updated each time the trajectory is altered.

Error associated with a robotically performed DCA procedure is composed of case-specific and general system error. System error pertaining to the robotic system and drilling process (primarily composed of tracking error and error due to tool bending) is entered as a static value into the planning tool by the user. For the described robotic system, general system error has been previously determined to be approximately 0.05 mm. Case-specific errors are attributed to the error pertaining to the patient-to-image registration. Whilst a specific registration error cannot be determined until after the registration process, a prediction of target registration error

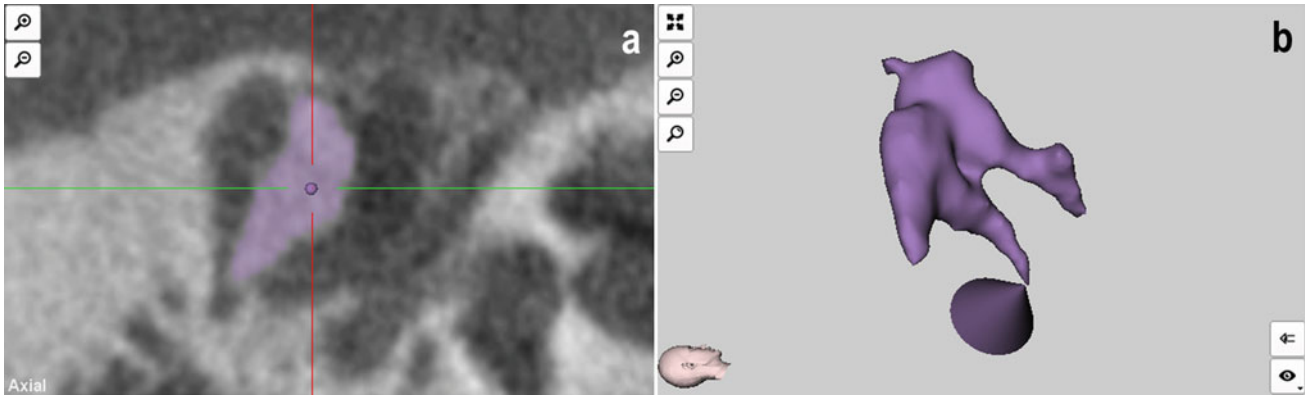

Fig. 7 Incus and malleus segmentation (**a**). 3D surface model of the incus, malleus and stapes (**b**)

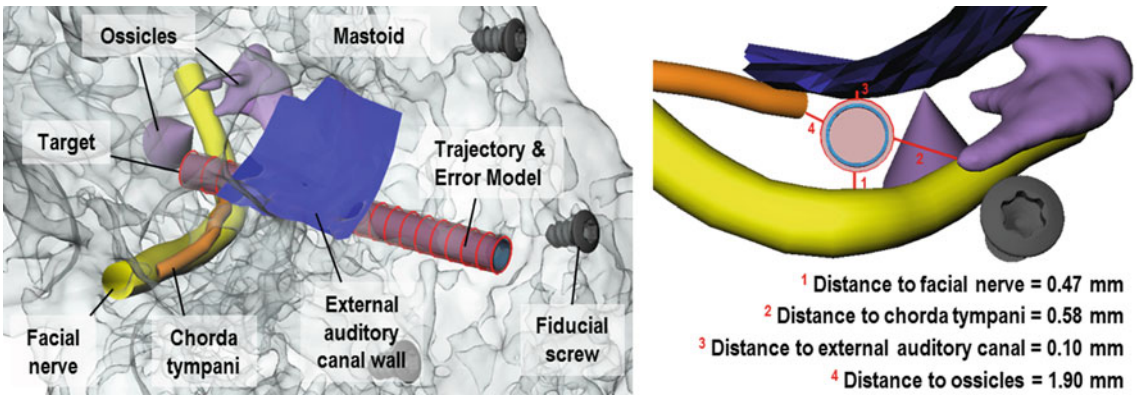

Fig. 8 Trajectory definition including minimum distances to structures

(TRE) can be approximated in the planning phase using equation (1) from Fitzpatrick et al. [18] where k is the number of dimensions, where d_k is the distance of the target from principal axis k of the fiducials, where f_k is the root mean square distance of the fiducials from principal axis k, where N is the number of fiducials and where FLE is a static value (0.159 mm) defined by the previously determined root mean square FLE associated with the employed fiducial detection methods within the image and on the patient [28].

$$\left\langle \mathrm{TRE}^2 \right\rangle \approx \frac{\left\langle \mathrm{FLE}^2 \right\rangle}{N} \left(1 + \frac{1}{3} \sum_{k=1}^{3} \frac{d_k^2}{f_k^2} \right) \tag{1}$$

where

$$\left\langle \mathrm{FLE}^2 \right\rangle = \left\langle \mathrm{FLE}_{\mathrm{im}}^2 \right\rangle + \left\langle \mathrm{FLE}_{\mathrm{pat}}^2 \right\rangle$$

Because registration error (TRE) varies with distance from the registration plane, the predicted value is calculated at 1 mm increments along the user selected trajectory. The total error value, defined as the addition of system error and predicted registration error for each increment, is calculated and displayed around the trajectory in the 3D model view. Additionally, distances to anatomical structures are computed including total error and are displayed to the user (see Fig. 8).

Verification

The proposed surgical planning approach was evaluated in robotically assisted DCA procedures using ten ears from five whole cadaver heads. For each ear, four fiducial screws were implanted prior to CBCT imaging (ProMax 3D Max, Planmeca, Finland) in high-resolution mode (0.15 mm × 0.15 mm × 0.15 mm). For each ear, a trajectory of ∅1.8 mm was planned from the mastoid surface to the middle of the round window through the facial recess with the objective of preserving all vital anatomical structures. Because of the importance of the facial nerve, any case in which it was not possible to define a trajectory with safety margin (from the tunnel to the facial nerve surface) greater than 0.2 mm was classified as ineligible for a DCA procedure and automatically excluded from the study. The time to create each of the ten plans was recorded. Each plan was imported into the image-guided robotic system and used for registration and guidance of the DCA procedure.

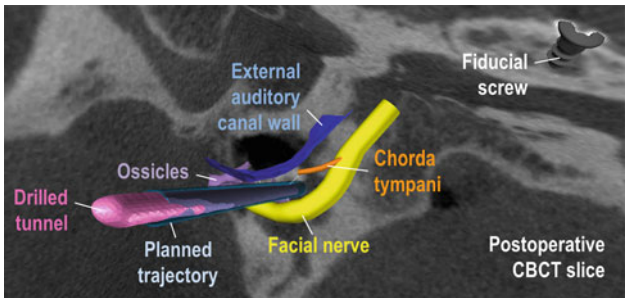

Fig. 9 Drilling results with drilled trajectory overlaid with preoperative plan

Postoperatively, a ∅1.8 mm titanium Kirschner wire was inserted into the drilled tunnels, and a CBCT image in high-resolution mode was acquired. On the resulting postoperative image data, the wire was segmented using region growing by selecting voxel intensities greater than 2500 HU. Linear least squares regression was used on the segmented voxels to find the axis of the DCA tunnel. Pair point matching was used to register the postoperative image data to the preoperative image data using the fiducial screw positions extracted with the proposed planning software system. The deviation of entrance was determined by computing the Euclidian distance between the planned entrance position and its projection onto the drilled trajectory axis. Similarly, the target deviation was obtained by computing the Euclidian distance between the planned target position and its projection onto the drilled trajectory axis. In order to verify the segmentation, the postoperative images were additionally examined visually for the presence of damage to vital structures.

Results

The proposed planning software system was successfully used to plan the ten DCA procedures. One head was found to have insufficient safety margins on both sides and was thus excluded from the study. Feedback from the software revealed that it was impossible to define a tunnel without penetrating both the facial nerve and the external auditory canal on the left side and that, on the right side, safety margins (including predicted errors) greater than 0.15 mm to the facial nerve were not possible. For eight of the ten ears, trajectories were planned to pass through the facial recess avoiding all vital anatomical structures (see Fig. 9).

The planning software did not predict damage to any vital structure for any of the eight DCA procedures. The plan for each ear was completed in less than 20 min with an average of approximately 16 min (N = 10, see Table 1).

Accurate DCA drilling was enabled via the presented dedicated fiducial detection algorithm in the image and resulted in mean drilling errors at the entrance and at the target of 0.08 ± 0.05 mm ($N = 8$) and 0.15 ± 0.08 mm ($N = 8$), respectively [31]. Through visual inspection of the postoperative images, it was observed that all vital anatomy was preserved in all eight DCA procedures and thus predicted safety margins for all cases were sufficient.

Table 1 Overview of preoperative planning time using the proposed software planning system

Cadaver head ID	Side	Preoperative planning time (min)
1	Right	16.13
	Left	14.20
2	Right	17.67[a]
	Left	19.30[a]
3	Right	12.68
	Left	14.50
4	Right	19.60
	Left	12.72
5	Right	19.80
	Left	12.87
Average: 15.95		

[a] Were found to have insufficient safety margins and were thus excluded from the study

Discussion

Within this work, we propose a dedicated surgical planning software tool for robotically performed DCA that enables safe trajectory planning and sufficiently accurate patient-to-image registration. Results of this study demonstrated that the software could aid in the safe planning of a DCA tunnel with an acceptable preoperative time. In addition, it provided fiducial localisation accuracy that enabled an overall procedure error of less than 0.26 mm and enabled procedures to be performed without damage to any vital anatomical structure.

Additionally, it is expected that the proposed planning software system would aid in the determination of a patient's eligibility for robotic DCA implantation. With very small distances between the drilled trajectory and critical anatomical structures, the ability of the surgeon to successfully assess the safety of the procedure and the eligibility of each patient is vital. Eligibility is primarily based on the expected error of the procedure and on the size of the facial recess through which the drilling trajectory passes. By providing a 3D visualisation of the internal anatomy, surgical plan and predicted surgical error and by displaying a quantitative analysis of predicted safety margins, the proposed planning software system aids the surgeon in this process. The definition of a general "sufficient" safety margin for an individual anatomical structure is not possible. The importance of preservation

of structures such as the chorda tympani or ossicles is, for example, additionally influenced by local customs or regulations and the presence of residual hearing, respectively, and thus must be determined by the operating surgeon for each individual case. It is thus believed that providing surgeons with useful, interpretable information regarding the predicted surgical situation within the planning phase and enabling them, with their extensive knowledge and experience, to make decisions regarding procedure safety, remains an optimal solution, superior to any fully automatic procedure planning algorithm or safety determination.

Additionally, due to small safety margins, the accuracy of the segmentation of anatomical structures throughout the planning process is paramount. Currently, the gold standard in segmentation is achieved through manual segmentation [32]. Unfortunately, integration of manual segmentation of all structures required for a DCA plan in clinical routine is not feasible due to the time involved. The proposed planning software system has been designed to increase the speed of the segmentation process whilst preserving the surgeons control over segmentation margins and their knowledge of the segmentation quality. Whilst fully automatic segmentation tools such as that described by Nobel et al. [14] reduce the interaction time, all feedback pertaining to the quality of the images and thus the segmentation is removed. Moreover, in order to maintain safety control over the procedure, it is important that the surgeon knows if structures have been over or, more importantly, under segmented. By involving the surgeon in the planning process and by displaying visualisations of segmentation regions to the user on standard image planes, verification of the segmentation can be conducted throughout the segmentation process.

The verification of segmentation and surgical planning software in general remains a challenge, especially due to the subjective nature of structure boundaries within a medical image. Within this study, the plan has been verified through the visualised preservation of anatomical structures on the postoperative CBCT data because this is the measure of success for such a planning tool. Future studies evaluating the segmentation accuracy in addition to the intra- and inter-segmentation variance using the presented semiautomatic methods will aim to further assess the quality of the segmentations through cross-examinations by qualified users.

Whilst the proposed planning software system currently aids the surgeon in constructing a safe and effective plan and in determining patient-specific eligibility for robotically assisted DCA, intraoperative error can never be completely predicted. For this reason, error predictions in the planning software provide only an approximate of drill positioning uncertainty and should thus be coupled with intraoperative error prediction methods that can be conducted after patient-to-image registration and throughout the drilling process. For example, error prediction can be reconfirmed after registration using matching error results and a technique, which correlates the drilling force history with bone density data to predict a tool's position within a porous structure like the mastoid [33], can be employed to continually reassess error during drilling.

In addition to interfacing with robotic systems, the proposed planning software system could support the planning of conventional hearing aid implantations, where patient-specific anatomy could be displayed in a 3D environment to increase the surgeon's spatial awareness.

Whilst this work focuses on the planning of the safe conduction of a DCA procedure for gaining access of the middle ear cavity, additional functionality that would aid in the implantation of a specific hearing device will be considered and integrated in future work. For example, the determination of a trajectory, approximately tangential to the basal turn of the cochlea, could aid to reduce trauma during the insertion of a cochlear implant electrode, and functionality for the planning of a device bed will be required for the positioning of more complex devices such as the DACS.

Conflict of interest None.

References

1. Häusler R (2002) Cochlear implantation without mastoidectomy: the pericanal electrode insertion technique. Acta oto-laryngologica 122(7):715–719
2. Kronenberg J, Baumgartner W, Migirov L, Dagan T, Hildesheimer M (2004) The suprameatal approach: an alternative surgical approach to cochlear implantation. Otol Neurotol 25(1):41–44 (discussion 44–45)
3. Warren FM, Balachandran R, Fitzpatrick JM, Labadie RF (2007) Percutaneous cochlear access using bone-mounted, customized drill guides demonstration of concept in vitro. Otol Neurotol 28(3):325–329
4. Schipper J, Aschendorff A, Arapakis I, Klenzner T, Teszler CB, Ridder GJ, Laszig R (2004) Navigation as a quality management tool in cochlear implant surgery. J Laryngol Otol 118(10):764–770
5. Labadie RF, Chodhury P, Cetinkaya E, Balachandran R, Haynes DS, Fenlon MR, Jusczyzck AS, Fitzpatrick JM (2005) Minimally invasive, image-guided, facial-recess approach to the middle ear: demonstration of the concept of percutaneous cochlear access in vitro. Otol Neurotol 26(4):557–562
6. Balachandran R, Mitchell JE, Blachon G, Noble JH, Dawant BM, Fitzpatrick JM, Labadie RF (2010) Percutaneous cochlear implant drilling via customized frames: an in vitro study. Otolaryngol Head Neck Surg Off J Am Acad Otolaryngol Head Neck Surg 142(3):421–426
7. Labadie RF, Mitchell J, Balachandran R, Fitzpatrick JM (2009) Customized, rapid-production microstereotactic table for surgical targeting: description of concept and in vitro validation. Int J Comput Assist Radiol Surg 4(3):273–280
8. Majdani O, Thews K, Bartling S, Leinung M, Dalchow C, Labadie R, Lenarz T, Heidrich G (2009) Temporal bone imaging: comparison of flat panel volume CT and multisection CT. AJNR Am J Neuroradiol 30(7):1419–1424
9. Klenzner T, Ngan CC, Knapp FB, Knoop H, Kromeier J, Aschendorff A, Papastathopoulos E, Raczkowsky J, Wörn H, Schipper J

(2009) New strategies for high precision surgery of the temporal bone using a robotic approach for cochlear implantation. Eur Arch Otorhinolaryngol 266(7):955–960
10. Baron S, Eilers H, Munske B, Toennies JL, Balachandran R, Labadie RF, Ortmaier T, Webster RJ (2010) Percutaneous inner-ear access via an image-guided industrial robot system. Proc Inst Mech Eng Part H J Eng Med 224(5):633–649
11. Noble JH, Majdani O, Labadie RF, Dawant B, Fitzpatrick JM (2010) Automatic determination of optimal linear drilling trajectories for cochlear access accounting for drill-positioning error. Int J Med Robot 6(3):281–290
12. Rodt T, Ratiu P, Becker H, Bartling S, Kacher DF, Anderson M, Jolesz F a, Kikinis R (2002) 3D visualisation of the middle ear and adjacent structures using reconstructed multi-slice CT datasets, correlating 3D images and virtual endoscopy to the 2D cross-sectional images. Neuroradiology 44(9):783–790
13. Jun B-C, Song S-W, Cho J-E, Park C-S, Lee D-H, Chang K-H, Yeo S-W (2005) Three-dimensional reconstruction based on images from spiral high-resolution computed tomography of the temporal bone: anatomy and clinical application. J Laryngol Otol 119(9):693–698
14. Noble JH, Dawant BM, Warren FM, Labadie RF (2009) Automatic identification and 3D rendering of temporal bone anatomy. Otol Neurotol 30(4):436–442
15. Jang HG, Chung MS, Shin DS, Park SK, Cheon KS, Park HS, Park JS (2011) Segmentation and surface reconstruction of the detailed ear structures, identified in sectioned images. Anat Rec (Hoboken, NJ: 2007) 294(4):559–564
16. Ma Z, Tavares JMRS, Jorge RN, Mascarenhas T (2010) A review of algorithms for medical image segmentation and their applications to the female pelvic cavity. Comput Methods Biomech Biomed Eng 13(2):235–246
17. Ferreira A, Gentil F, Tavares JM (2012) Segmentation algorithms for ear image data towards biomechanical studies. Comput Methods Biomech Biomed Eng PP 1–17
18. Fitzpatrick JM, West JB, Maurer CR (1998) Predicting error in rigid-body point-based registration. IEEE Trans Med Imaging 17(5):694–702
19. Schermeier O, Lueth T, Glagau J, Szymanski D, Tita R, Hildebrand D, Klein M, Nelson K, Bier J (2002) Automatic patient registration in computer assisted maxillofacial surgery. Stud Health Technol Inform 85:461–467
20. Labadie RF, Shah RJ, Harris SS, Cetinkaya E, Haynes DS, Fenlon MR, Juscyzk AS, Galloway RL, Fitzpatrick JM (2004) Submillimetric target-registration error using a novel, non-invasive fiducial system for image-guided otologic surgery. Comput Aided Surg Off J Int Soc Comput Aided Surg 9(4):145–153
21. Wang MY, Maurer CR, Fitzpatrick JM, Maciunas RJ (1996) An automatic technique for finding and localizing externally attached markers in CT and MR volume images of the head. IEEE Trans Bio-med Eng 43(6):627–637
22. Gu L, Peters T (2004) 3D Automatic fiducial marker localization approach for frameless stereotactic neuro-surgery navigation morphological treatment for the detection of fiducial markers. In: MIAR 2004, vol LNCS 3150, pp 329–336
23. Krishnan R, Hermann E, Wolff R, Zimmermann M, Seifert V, Raabe A (2003) Automated fiducial marker detection for patient registration in image-guided neurosurgery. Comput Aided Surg Off J Int Soc Comput Aided Surg 8(1):17–23
24. Maurer CR, Fitzpatrick JM, Wang MY, Galloway RL, Maciunas RJ, Allen GS (1997) Registration of head volume images using implantable fiducial markers. IEEE Trans Med Imaging 16(4):447–462
25. Maurer CR, Fitzpatrick JM, Wang MY, Maciuna RJ (1993) Estimation of localization accuracy for markers in multimodal volume images. In: Proceedings of the 15th annual international conference of the IEEE engineering in medicine and biology societ, vol Im, no 2, pp 124–125
26. Wang M, Song Z (2008) Automatic detection of fiducial marker center based on shape index and curvedness. In: MIAR 2008, vol LNCS 5128, pp 81–88
27. Bell B, Stieger C, Gerber N, Arnold A, Nauer C, Hamacher V, Kompis M, Nolte L, Caversaccio M, Weber S (2012) A self-developed and constructed robot for minimally invasive cochlear implantation. Acta oto-laryngologica 132(4):355–360
28. Gerber N, Gavaghan K, Bell B, Williamson T, Weisstanner C, Caversaccio M, Weber S (2013) High accuracy patient-to-Image registration for the facilitation of image guided robotic microsurgery on the head. IEEE Trans Bio-med Eng 60(4):960–968
29. Lorensen WE, Cline HE (1987) Marching cubes: a high resolution 3D surface construction algorithm. Comput Graph 21(4):163–169
30. Kanitsar A, Fleischmann D, Wegenkittl R, Felkel P, Gröller ME (2002) CPR-curved planar reformation. In: IEEE visualization, 2002 (VIS 2002), pp 37–44
31. Bell B, Gerber N, Williamson T, Gavaghan KA, Wimmer W, Caversaccio M, Weber S (2013) In vitro accuracy evaluation of image-guided robot system for direct cochlear access. Otol Neurotol (in press)
32. Olabarriaga SD, Smeulders AW (2001) Interaction in the segmentation of medical images: a survey. Med Image Anal 5(2):127–142
33. Williamson TM, Bell BJ, Gerber N, Salas L, Zysset P, Caversaccio M, Weber S (2013) Estimation of tool pose based on force-density correlation during robotic drilling. IEEE Trans Bio-med Eng 60(4):969–976